

Christian-Albrechts-Universität zu Kiel

Bachelor thesis

The influence of spin-orbit-coupling on the
electronic properties of Molybdenum
ditelluride

by Neil Matzen

Contents

1	Introduction	1
2	Motivation	2
3	Theory	4
3.1	Density functional theory	4
3.1.1	Hohenberg-Kohn theorem	6
3.1.2	Kohn-Sham equations	8
3.1.3	Bloch function	10
3.1.4	Self-consistent-field-method calculation	12
3.2	Spin-orbit coupling	13
3.3	Spin-orbit coupling induced band splitting	15
3.3.1	Dresselhaus splitting	17
3.3.2	Rashba splitting	18
4	Quantum Espresso	19
5	Results	21
5.1	<i>Td</i> – <i>MoTe₂</i>	21
5.2	Convergence	23
5.2.1	Energy cut off	23
5.2.2	Automatic k-points	25
5.3	Pseudopotential	27
5.4	Band structure and spin-orbit coupling	28
5.5	Intensities of the bands	31
5.6	Effect of displacement	33
6	Conclusion/Outlook	37
7	References	39
8	Appendix	41
8.1	Basic SCF input file	41
8.2	Basic NSCF input file	42
8.3	Code used to calculate the bandstructure with intensities	43
9	Selbstständigkeitserklärung	45

List of Figures

1	Model of a three layer WTe bulk crystal with inter layer sheer mode excitation	2
2	Basic pattern of a self-consistent-field-method calculation	12
3	Spin-orbit-coupling basic idea	13
4	Example of band splitting in a 3-dimensional semiconductor	15
5	Spin structure of Dresselhaus splitting	17
6	Spin structure of Rashba splitting	18
7	Td-MoTe2 bulk crystal structure	21
8	1st brillouinzone of Td-MoTe2 with k-path	21
9	Bandstrucutre of MoTe2 along the k-path shown in the previous figure . .	22
10	Energy cut off in the input file	23
11	Convergence of the energy cut off	24
12	Automatic k-points in the input file	25
13	Convergence of the Automatic k-points	25
14	Toggling spin-orbit coupling in the input file	28
15	Bandstructure plot with spin-orbit coupling disabled	28
16	Bandstructure plot with spin-orbit coupling enabled	29
17	Bandstructure plot close up with spin-orbit coupling disabled	29
18	Bandstructure plot close up with spin-orbit coupling enabled	30
19	Experimental bandstructure	31
20	The basic course of a Lorentzian function	32
21	Lorentzian function applied on the bandstructure	32
22	Position of the atoms in the input file	33
23	Position of the atoms in the input file - with displaced atoms	33
24	Band observed in the displacement process	34
25	Energy changes caused by the displacement of the atoms	34

List of Tables

1 Kinetic energy cut off relative to total energy 24

1 Introduction

In the last few decades, spin-orbit coupling has been of great importance in solid state physics[10]. Due to the research of many scientists, especially Gene Dresselhaus[12] and Emmanuel Rashba[13], new discoveries concerning the behavior of electron bandstructures and spin-orbit coupling have been made.

The main subject of this thesis is to see and analyze the effect of spin-orbit coupling on the electronic properties of Molybdenum ditelluride (MoTe₂). By analyzing the bandstructure of MoTe₂ the electronic properties and their changes, due to spin-orbit coupling, can be derived.

The bandstructure calculation is done using a density functional theory based approach. That is why in the theory section the first few chapters discuss the approach in density functional theory thoroughly. Since the spin-orbit coupling and its effects are primarily investigated, the basic theory of spin orbit coupling and the spin-orbit coupling induced bandsplitting are explained in the theory section as well.

Next to explaining relevant theoretical topics, a few convergence based assumptions must be done, so that accurate results can be achieved. After doing all these considerations the bandstructures are analyzed to determine the effects of spin-orbit coupling on the basic bandstructure of MoTe₂. The next step is an intermediate step, which doesn't concern the spin-orbit coupling specifically but is still relevant for the bandstructure of the MoTe₂: Recreating intensities of the bandstructure, that are found in experimental bandstructures by using a suitable function. Lastly the experiment from the "Motivation" section is recreated by simulating the phonon excitation through displacement of the atoms in the calculations.

After performing all steps the influence of spin-orbit coupling on the electronic properties of MoTe₂ will be clear to a certain extend.

2 Motivation

The topic of this thesis is motivated by the article: Hein, P., Jauernik, S., Erk, H. et al. Mode-resolved reciprocal space mapping of electron-phonon interaction in the Weyl semimetal candidate Td-WTe₂. Nat Commun 11, 2613 (2020)[1].

By stimulating the phonons and evaluating the bandstructure of a Tungsten ditelluride (WTe₂) bulk crystal, they analysed the electron-phonon interaction. The stimulation of the phonons was achieved by using an 827nm high frequency laser on the sample. Since the material is a bulk crystal consisting of stacked WTe₂ layers that are bound by van der Waals interaction, the excitation of the phonons results in an interlayer sheer mode excitation. As shown in the figure below, the top and bottom layers shift to the right, while the middle layer shifts into the other direction.

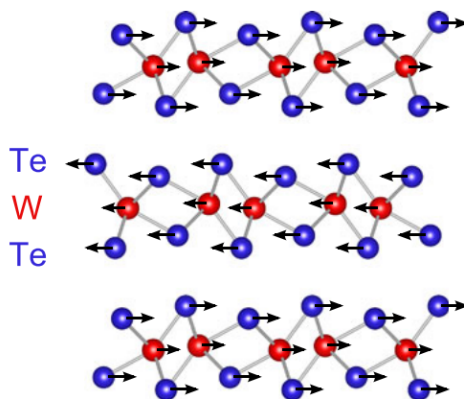


Figure 1: Model of a three layer WTe₂ bulk crystal. The arrows indicate a displacement of the atoms due to the excitation of the phonons. In this case the excitation is specifically called interlayer sheer mode excitation, because the interlayer is displaced in a different direction than the outer layers. This figure was taken from refernce[1]

Without the excitation of the bulk the WTe₂ has a Td-WTe₂ structure, a non centrosymmetric structure, which exists in the groundstate. By exciting the material the symmetry of the structure changes and the material makes a structural phase transition to a centrosymmetric state, that is called 1T'-WTe₂. The change in symmetry has a measurable effect on the bandstructure.

For this thesis instead of WTe₂, the material that was considered, was Molybdenum ditelluride. The reason is, that the material has very similar properties to WTe₂, above all the lattice structure of WTe₂ and MoTe₂ are almost the same and therefore a similar behavior of the material is to be expected[2].

3 Theory

3.1 Density functional theory

The following section is based on the book Giustino, Feliciano. Materials Modelling Using Density Functional Theory : Properties and Predictions, Oxford University Press, 2014., specifically the chapter "Many-body Schrödinger equation"[4].

Density functional theory (DFT) is a concept to simplify the mathematical approach on calculating the properties of a many electron system. To establish this concept, the single particle Schrödinger equation is the starting point.

$$\left(\frac{p^2}{2m_e} + v(r)\right)\Phi(r) = E_{tot}\Phi(r) \quad (1)$$

In order to consider all electrons the equation has to be extended by utilizing the many-body wavefunction $\Psi = \Psi(r_1, r_2, \dots; r_n; R_1, R_2, \dots, R_m)$. Applying this wavefunction on the single particle Schrödinger equation the many body Schrödinger equation is derived:

$$(E_{kin} + E_{pot})\Psi = E_{tot}\Psi \quad (2)$$

Next up is the Hamiltonian of the electrons. A single electron Hamiltonian

$$\mathcal{H} = -\frac{1}{2}\nabla^2 + V_n(r) \quad (3)$$

is not enough to describe the system, since just suming up all the single particle Hamiltonians does not satisfy the interaction between the electrons themselves. Therefore the interaction, defined by the coulomb potential, has to be included. After making these considerations, the many electron Hamiltonian is:

$$\mathcal{H}(r_1, \dots, r_n) = -\sum_i \frac{1}{2}\nabla_i^2 + \sum_i V_n(r_i) + \frac{1}{2}\sum_{i \neq j} \frac{1}{|r_i - r_j|} \quad (4)$$

The total energy is calculated from the many electron Hamiltonian, as well as the many-body Schrödinger equation and is defined by:

$$E = \langle \psi | H | \Psi \rangle \quad (5)$$

$$(6)$$

Since the many electron Hamiltonian does not consider the material, any changes in E must depend changes in our many body wave function. That concludes: E is a functional of Ψ . To get from the many body Schrödinger equation to the DFT it must be proven, that E is a functional of the electron density. This only applies for the lowest energy

state of the total energy and is explained in more detail in the next chapter. The main advantage of using DFT is the simplification of the model resulting in equations, that can be calculated relatively easy by a computer. The disadvantage is, that only the lowest energy state, also called ground state, can be considered. An excitation of the state results in E not being a functional of the electron density anymore. Any excited states must therefore be calculated based on a more complex and difficult to solve base.

3.1.1 Hohenberg-Kohn theorem

The following section is based on the physical review P. Hohenberg and W. Kohn: Inhomogeneous Electron Gas. Phys. Rev. 136 (1964) B864-B871[3]

The fact, that the energy of the ground state is determined by the electron density, was discovered by Hohenberg and Kohn in 1964. They made a three step connection between the electron density of a system and the energy of the ground state.

The first step is to show, that the external potential $v(r)$ has to be a functional of the electron density in the ground state.

The electron density is

$$n = \langle \Psi | \psi^* \psi | \Psi \rangle \quad (7)$$

and therefore a functional of the external potential $v(r)$.

Now to proof, that there's a unique density $n(r)$ for each potential $v(r)$ the following contradiction serves as proof:

Assuming there are two external potentials $u(r)$ and $v(r)$ for the same electron density

$$u(r) \neq v(r), \quad (8)$$

then there must be two ground states Ψ' and Ψ

$$\Psi' \neq \Psi \quad (9)$$

and two Hamiltonians

$$H = T + U + V \quad (10)$$

$$H' = T + U + V' \quad (11)$$

$$H \neq H' \quad (12)$$

The two ground states E and E' can be written as

$$E = \langle \Psi | H | \Psi \rangle \quad (13)$$

$$E' = \langle \Psi' | H' | \Psi' \rangle \quad (14)$$

By definition of the ground state being the lowest state possible the following equations are obvious:

$$E = \langle \Psi | H | \Psi \rangle < \langle \Psi' | H | \Psi' \rangle = \langle \Psi' | H' + V - V' | \Psi' \rangle = E' + \langle \Psi' | V - V' | \Psi' \rangle \quad (15)$$

$$E' = \langle \Psi' | H' | \Psi' \rangle < \langle \Psi | H' | \Psi \rangle = \langle \Psi | H + V' - V | \Psi \rangle = E + \langle \Psi | V' - V | \Psi \rangle \quad (16)$$

$$(17)$$

Since the electron densities are equal for both cases:

$$\langle \Psi | V' - V | \Psi \rangle = \langle \Psi' | V - V' | \Psi' \rangle = C \quad (18)$$

This results in two different equations:

$$E < E' + C \quad (19)$$

$$E' < E + C \quad (20)$$

Therefore the claim is falsified and the statement, that there is a unique density for every external potential, is proven.

The next step is to show, that the many body wave function is a functional of the external potential. Since changing the atomic species or changing the atomic positions, in other words changing the external potential, will result in a change of the many body wave function. Therefore no further proof has to be made and the external potential has to uniquely determine the many body wave function.

The last step is to show, that the total energy is a functional of Ψ . This has already been done by defining the total energy and the many electron Hamiltonian:

$$E = \int dr_1 \dots dr_n \Psi + (r_1, \dots, r_n) \mathcal{H} \Psi(r_1, \dots, r_n) \quad (21)$$

$$\mathcal{H}(r_1, \dots, r_n) = - \sum_i \frac{1}{2} \nabla_i^2 + \sum_i V_n(r_i) + \frac{1}{2} \sum_{i \neq j} \frac{1}{|r_i - r_j|} \quad (22)$$

As mentioned before, the many electron Hamiltonian is not influenced by any changes in the material, resulting in E being a functional of Ψ .

After doing these three steps, it is proven, that the total energy of the ground state is a functional of the electron density.

3.1.2 Kohn-Sham equations

The following section is based on the book Giustino, Feliciano. Materials Modelling Using Density Functional Theory : Properties and Predictions, Oxford University Press, 2014., specifically the chapter "Density functional theory" [4]

While the Hohenberg-Kohn theorem was about proving the concept of the electron density being a functional of the total energy, the Kohn-Sham equations focus on developing a functional that is utilized to perform DFT calculations.

Proven in the last chapter was, that the total energy is a functional of the electron density:

$$F[n] = E \quad (23)$$

Further that means, the functional of the electron density can be written dependent on the many electron Hamiltonian and the many body wave function.

$$F[n] = \langle \psi | H | \Psi \rangle = \langle \psi | T + U + V | \Psi \rangle \quad (24)$$

$$= \int dr n(r) V_n(r) - \sum_i \int dr \Psi_i^*(r) \frac{\nabla^2}{2} \psi_i(r) + \frac{1}{2} \int \int dr dr' \frac{n(r)n(r')}{|r - r'|} + E_{xc}[n] \quad (25)$$

The E_{xc} is the so called "exchange and correlation energy", which is unknown. Apart from the exchange and correlation energy, which is considered to be relatively low, the only unknown aspect of the equation is the electron density. The other parts of the equation are:

$$\text{External potential} = \int dr n(r) V_n(r) \quad (26)$$

$$\text{Kinetic energy} = - \sum_i \int dr \Psi_i^*(r) \frac{\nabla^2}{2} \psi_i(r) \quad (27)$$

$$\text{Hartree energy} = \frac{1}{2} \int \int dr dr' \frac{n(r)n(r')}{|r - r'|} \quad (28)$$

Utilizing the external potential, kinetic energy, Hartree energy and the exchange correlation energy in the Schrödinger equation, the Kohn Sham equations can be derived:

$$\left[-\frac{1}{2} \nabla^2 + V_n(r) + V_H(r) + V_{xc}(r) \right] \phi_i = E_i \phi_i \quad (29)$$

In the Kohn Sham equations the Hartree potential is given through the poisson equation as:

$$\nabla^2 V_H(r) = -4\pi n(r) \quad (30)$$

The exchange and correlation potential is defined as:

$$V_{xc}(r) = \frac{\delta E_{xc}}{\delta n(r)} \quad (31)$$

Now, that everything has been defined, the equations are still quite far from being solvable, since the electron density, as well as the exchange and correlation potential are still unknown.

3.1.3 Bloch function

The following section is based on Kopitzki K., Herzog, P., Einführung in die Festkörperphysik, Springer-Verlag GmbH Deutschland, 2017, page 115-116 [5]

Prior to solving the Kohn-Sham equations the exact solution of the wave function has to be determined. To explain this it is easier to make use of the Schrödinger equation for a single electron:

$$\left(\frac{1}{2}\nabla^2 + V_{eff}\right)\Psi = E\Psi \quad (32)$$

The Potential $V_{eff}(r)$ in this equation does not change if a geometrical translation is applied. That specifies, that the wave functions $\Psi(r)$ and $\Psi(r + R)$ are connected by:

$$f(R)\Psi(r) = \Psi(r + R) \quad (33)$$

Looking at two different geometric translations R_k and R_l , the following terms can be written as equal:

$$\Psi(r + R_k + R_l) = f(R_k)\Psi(r + R_l) = f(R_l)\Psi(r + R_k) = f(R_l)f(R_k)\Psi(r) = f(R_l + R_k)\Psi(r) \quad (34)$$

To satisfy these equations, the function $f(x)$, must be an exponential function in the form:

$$f(x) = e^{ikx} \quad (35)$$

Exchanging the $f(x)$ with the exponential function results in:

$$\Psi(r + R_k + R_l) = e^{R_k}\Psi(r + R_l) = e^{R_l}\Psi(r + R_k) = e^{R_l}e^{R_k}\Psi(r) = e^{R_l+R_k}\Psi(r) \quad (36)$$

$$\Psi(r + R_k + R_l) = e^{R_k}\Psi(r + R_l) = e^{R_l}\Psi(r + R_k) = e^{R_l+R_k}\Psi(r) = e^{R_l+R_k}\Psi(r) \quad (37)$$

That means for any geometrical translation the translation of the wave function is defined by:

$$\Psi(r + R) = \Psi(r)e^{ikR} \quad (38)$$

The equation above is the Bloch theorem. A Schrödinger equation with a periodical potential must fulfill this potential and because periodical structures, like crystal structures, are used. Due to the Bloch function, the wave function has to be:

$$\Psi(r) = u_k(r)e^{ikr} \quad (39)$$

where $u_k(r) = u_k(r+R)$. This function for $\Psi(r)$ can now be solved for every k individually and be used to calculate for example the electron density.

3.1.4 Self-consistent-field-method calculation

The Self-consistent-field-method (SCF) is utilized to calculate the total energy. To do this the calculation behaves like in the figure shown below.

First an initial guess on the electron density is made. This electron density is used to calculate the Hartree-potential and the Exchange and correlation potential.

The next step is to calculate the effective potential and a new electron density.

The difference between the new values and the former values is compared to a certain threshold value.

If the difference is larger, the electron density is used to start the process again. If the difference is smaller the calculated values are within the range of error that is acceptable and can be used for further calculations.

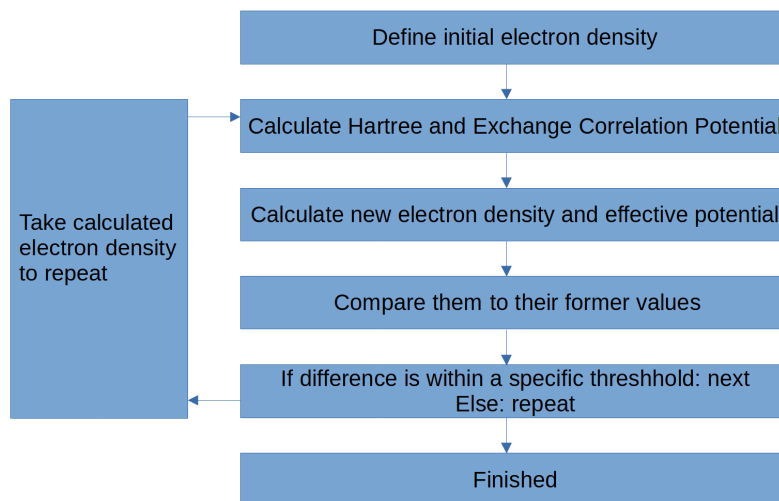


Figure 2: Basic pattern of a self-consistent-field-method calculation.

Even though the accuracy can be greatly increased by defining a very small threshold value, the time consumption of the calculation will increase drastically. Therefore the threshold can't be too small. Although, to give an example, the threshold used in the calculation, performed in this thesis, is about 10^{-12} and the estimated accuracy at around $5 \cdot 10^{-12}$ Ry. Compared to other sources of error this is incredibly small.

3.2 Spin-orbit coupling

The following section is based on the book Dresselhaus, M.S., Dresselhaus, G., Jorio, A.. Group Theory: Application to the Physics of Condensed Matter, 337,(2008) [7].

Spin-orbit-coupling is an interaction that can be described in a relatively easy manner. The electron itself has a magnetic moment induced by the electron spin. It also moves around the nucleus in circles, which creates an angular momentum. From the perspective of the electron, the angular momentum lies at the nucleus. Therefore the moving positive charge (nucleus) creates a magnetic field that interacts with the spin induced magnetic moment of the electron. This interaction is called spin-orbit coupling.

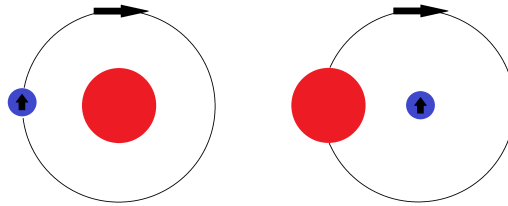


Figure 3: The basic idea of the spin orbit coupling shown in the bohr model. The red circles symbolizes the nucleus, the smaller blue circle stands for the the electron. The small arrow inside the electron represents the spin and the large arrow at the outer black circle indicates the orbital movement

To be able to describe the interaction mathematical the Hamiltonian \mathcal{H}_{SO} of the spin-orbit interaction needs to be determined. In general the Hamiltonian is given by:

$$\mathcal{H}_{SO} = -\mu \cdot H \quad (40)$$

The magnetic moment μ can be determined with the spin angular momentum S through the following equation:

$$\mu = -\frac{|e|\hbar}{mc} S \quad (41)$$

The magnetic field, that the electron experiences, can be described by Biot-Savart:

$$H = -\frac{v}{c} \times E \quad (42)$$

The electric field E , used in the previous equation, is generated by the crystal itself. Combining equations (38)-(40) the result is:

$$\mathcal{H}_{SO} = -\frac{|e|\hbar}{mc} S \frac{v}{c} \times E \quad (43)$$

In the next few steps the equation is reshaped without changing the content:

$$\mathcal{H}_{SO} = -\frac{|e|\hbar}{mc} S \cdot \frac{m}{\hbar} \times E \cdot \frac{\hbar}{m} \quad (44)$$

$$\mathcal{H}_{SO} = -\frac{|e|\hbar}{m^2 c^2} m v \times E \cdot S \quad (45)$$

$$\mathcal{H}_{SO} = -\frac{1}{m^2 c^2} p \times |e|\hbar E \cdot S \quad (46)$$

Using basic methods the following can be simplified:

$$|e|\hbar E = F = -\nabla V, \quad (47)$$

Here V is the potential energy of the magnetic field introduced by the nucleus. Because of relativistic effects a factor of $1/2$ has to be added. The Hamiltonian can now be written as:

$$\mathcal{H}_{SO} = -\frac{1}{2m^2 c^2} (p \times \nabla V) \cdot S \quad (48)$$

This Hamiltonian is part of the single electron Hamiltonian that describes an electron in a solid. To get the full Hamiltonian of the electron the kinetic energy and the external potential would need to be considered as well.

3.3 Spin-orbit coupling induced band splitting

The following section is based on the book Winkler R.. Spin–Orbit Coupling Effects in Two-Dimensional Electron and Hole Systems, p.69 ff., (2003) [8] and Lechner, V. Bulk and Structure Inversion Asymmetry in Semiconductor Quantum Well Structures, 9, (2012)[9]

Due to the previous discussed spin-orbit coupling a splitting of the electron bands, also called spin splitting, occurs.

In the following figure the splitting of the bands is shown in a simple configuration. CB, the conduction band is an s-type band with $l = 0$, therefore we don't expect any degeneracy. In the valence band, a p-type band in this case, with $l = 1$, the expected degeneracy would be $m_{l_1} = -1, m_{l_2} = 0$ and $m_{l_3} = 1$. Because of the spin orbit interaction, this is not the case. The angular momentum and the spin are not considered as two separate influences, but as a combined total angular momentum:

$$J = L + S \quad (49)$$

This results in two states, $j = 1/2$ and $j = 3/2$ instead of one $l = 1$. The heavy hole band(hh), with $m_j = \pm 3/2$, and the light hole band (lh), with $m_j = \pm 1/2$ at $j = 3/2$ as well as the split off band(so) with $m_j = \pm 1/2$ at $j = 1/2$. The gap between the split off band and the other two bands is the so called spin orbit gap.

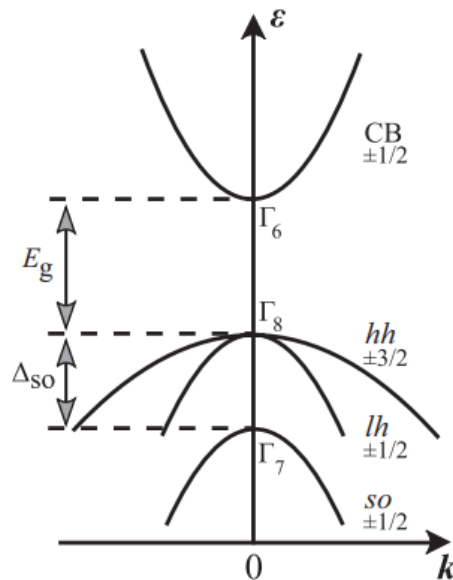


Figure 4: Example of band splitting in a 3-dimensional semiconductor. CB stands for conduction band, the other three bands heavyhole band (hh), lighthole band(lh) and the split off band (so) are all valence bands. This figure was taken from reference [9]

The degeneracy of the bands still isn't fully removed, the heavy hole band, the light

hole band and the split off band all still have a twofold degeneracy. The degeneracy in general is caused by inversion symmetry in space and time. The symmetries are given by the equations:

$$\text{Space inversion symmetry: } E_{\uparrow}(k) = E_{\uparrow}(-k), E_{\downarrow}(k) = E_{\downarrow}(-k) \quad (50)$$

$$\text{Time inversion symmetry : } E_{\uparrow}(k) = E_{\downarrow}(-k) \quad (51)$$

Combining them result in:

$$E_{\uparrow}(k) = E_{\downarrow}(k) \quad (52)$$

This inversion symmetry can be broken by applying a magnetic field, resulting in the so called Zeeman effect. Another way is to use a material, that has no inversion symmetry.

3.3.1 Dresselhaus splitting

The following section is based on the dissertation Lechner, V. Bulk and Structure Inversion Asymmetry in Semiconductor Quantum Well Structures, 9, (2012) [9].

The Dresselhaus splitting is a type of spin splitting caused by the inversion asymmetry of a bulk material (BIA) and fulfills the condition stated before. Therefore a material with a bulk inversion asymmetry causes a spin splitting of the states. The Dresselhaus splitting can usually be seen in zinc blende structures which have no center of inversion.

At the Γ -point the Dresselhaus splitting is generally expressed by the following term:

$$\mathcal{H} = \beta(k_x\sigma_x - k_y\sigma_y) + \gamma(-\sigma_x k_x k_y^2 + \sigma_y k_y k_x^2) \quad (53)$$

In the equation there is a linear, as well as a cubic term with k. The cubic term is often not considered because of the small effect in systems with a rather small spin orbit interaction. Instead of being dependent on the strength of a magnetic field, the Dresselhaus splitting is influenced by the crystal fields. Therefore it depends on the properties of the quantum well. To get a better understanding of the Dresselhaus splitting the spin-texture present at the splitting can be analyzed. The following figure is a schematic demonstration of the spin components relative to the wave vector.

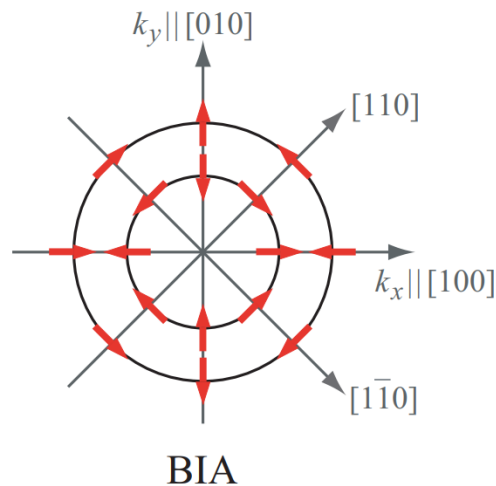


Figure 5: This figure shows a basic example of the spin texture in a solid with the Dresselhaus splitting present. This figure was taken from reference [9]

3.3.2 Rashba splitting

The following section is based on the dissertation Lechner, V. Bulk and Structure Inversion Asymmetry in Semiconductor Quantum Well Structures, 9, (2012) [9].

Instead of depending on a bulk inversion asymmetry the Rashba splitting is dependent on the structure inversion asymmetry (SIA). That means the Rashba splitting is influenced by the confining potential. In the figure below the estimated spin structure in presence of the Rashba effect can be observed.

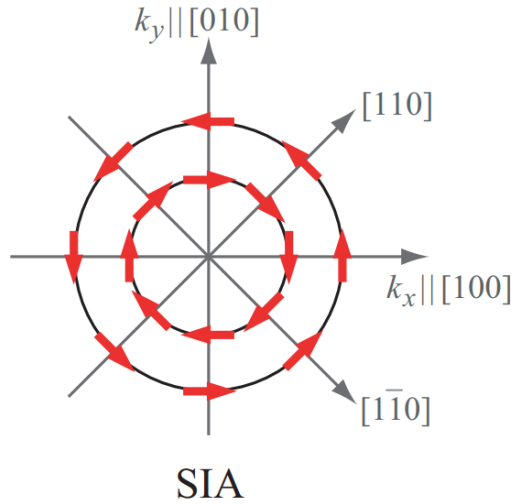


Figure 6: This figure shows a basic example of the spin texture in a solid with the Rashba splitting present. This figure was taken from reference [9]

The asymmetry of the crystal structure creates an electric field, as well as influences the wave function close to the nuclei. This results in the splitting of the bands and can be described by the following formula:

$$\mathcal{H} = \alpha(\sigma_x k_y - \sigma_y k_x) \quad (54)$$

The Dresselhaus splitting and the Rashba splitting can be present at the same time, either working against each other, or together. Unlike the Dresselhaus splitting, the Rashba splitting has been confirmed to affect the bandstructure of many different materials[10].

4 Quantum Espresso

Quantum Espresso is an open source software for calculating electronic structures in density functional theory. All DFT based calculations in this thesis were performed using Quantum Espresso.

To calculate a basic bandstructure, some prior calculations need to be performed. First of all an SCF calculation needs to be done. For that an input file is created, that contains all relevant information. This information contains information on the lattice, of the material, the atomic positions of the material, pseudopotentials, kinetic energy cut off, number of k-points and a lot more.

After doing the SCF calculation a non self consistent field method calculation (NSCF) is performed. The input file is basically the same, except that there is a path of k-points given. Instead of doing the same thing as the SCF calculation, the NSCF calculation calculates the energy for the k-points on the path, that shall be investigated. This path is usually defined by highsymmetry points of the crystal and is what is shown in the bandstructure.

As the last step, the data has to be extracted from the output file by utilizing a simple band extraction input file. This result in a file, that contains all bands, that were calculated in the NSCF calculation and can be easily plotted in a bandstructure.

For the calculations in this thesis, the parameters that were needed to work with the most, were the kinetic energy cutoff, automatic k-points, the k-points between the highsymmetry points and the spin-orbit-coupling.

The kinetic energy cutoff and the automatic k-points were changed to look at the convergence of the total energy and will be explained in more detail in the results.

By changing the number of k-points between the individual highsymmetry points the resolution of the plot can be influenced manually. This needs to be adjusted in order to fit the effects that is supposed to be observed.

The spin-orbit coupling can be turned on and of and therefore bandstructures with spin-orbit coupling neglected and considered later in the thesis can be compared.

5 Results

5.1 $Td - MoTe_2$

The material, used in the calculations, is Molybdenumditelluride ($MoTe_2$). It consists of two different species of atoms, Molybdenum, with an atomic number of 42 and Tellurium, with an atomic number of 52. The $MoTe_2$ is a structure that in this case was a bulk crystal that consists of mono layers of $MoTe_2$.

As visible in the figure below, the layers of $MoTe_2$ are bound by the van der Waals interaction. The $MoTe_2$ in this case is $Td-MoTe_2$, the ground state of the material.

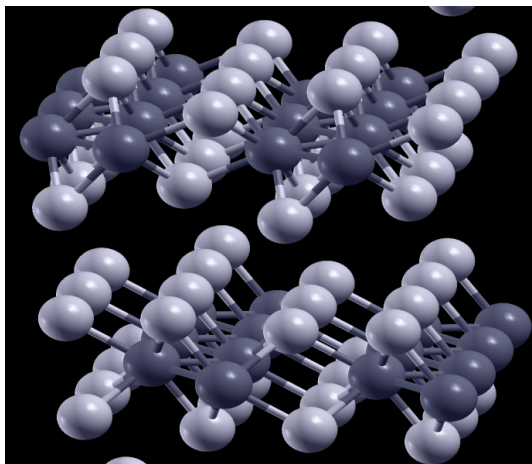


Figure 7: $Td-MoTe_2$ bulk crystal structure

The 1st Brillouin zone of $MoTe_2$ is shown in the next figure.

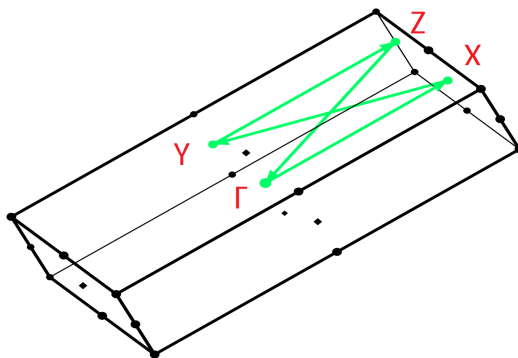


Figure 8: 1st Brillouin zone of $Td-MoTe_2$ with k-path

The green arrows indicate the k-path that was chosen along the high-symmetry points for the bandstructure and goes as follows:

$$\Gamma \rightarrow X \rightarrow Y \rightarrow Z \rightarrow \Gamma \quad (55)$$

For calculations later in the thesis only the path

$$\Gamma \rightarrow X \tag{56}$$

was considered due to problems in the calculation. After looking at the 1st brillouinzone and the k-path, a basic bandstructure of the Td-MoTe2 can be calculated.

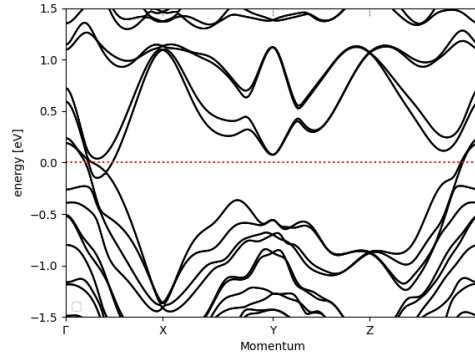


Figure 9: Bandstructure of MoTe2 along the k-path shown in the previous figure

There are bands crossing the fermi energy at the Γ , which indicates metallic properties of the material. The minimum energy of the highest valence band is found at the X-point. In the calculation spin-orbit coupling was already considered.

5.2 Convergence

5.2.1 Energy cut off

When calculating the wave function, the Bloch function, that was introduced earlier in the thesis, is utilized:

$$\Psi(r) = u_k(r)e^{ikr} \quad (57)$$

The factor $u_k(r)$ can be written as a sum of standing waves over every single lattice vector. This could be for example:

$$u_k(k) = \sum_R c_R e^{iRr} \quad (58)$$

That means trying to solve the wavefunction now is impossible, since the number of lattice vectors is simply too large.

Looking at the kinetic energy, the electrons further away from the nucleus, that have a smaller energy, are more relevant than the electrons closer to the nucleus. The energy can therefore be cut off for at a certain value, meaning, that the result won't be 100% accurate, but a total energy, that resembles the real value to a high degree. The calculation converges to a certain value and now the matter of interest is, at which energy cutoff the result is close enough to the actual total energy, that the accuracy of our calculation is satisfying.

```
&SYSTEM
  degauss = 0.02
  ecutwfc = 80
  ecutrho = 600
  ibrav = 0
  nat = 12
  nosym = .false.
  ntyp = 2
  occupations = 'smearing'
  smearing = 'cold'
  lspinorb = .true.
  noncolin = .true.
```

Figure 10: This figure shows the parameter of the energy cut off in the SCF and NSCF input file.

To achieve that, the SCF calculation has to be performed with a variation of the energy cut off parameter and plot the kinetic energy cut off relative to its total energy counterpart, as shown in the following figure below.

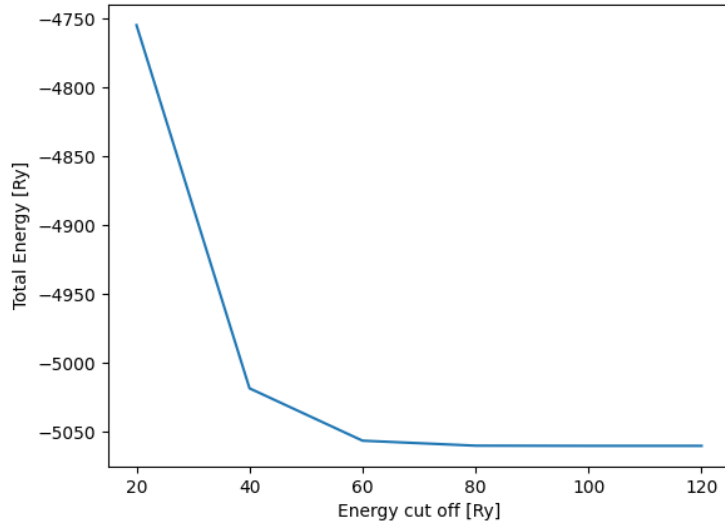


Figure 11: This figure shows the convergence of our calculated total energies, relative to the energy cut off.

The total energy in the plot converges at around 5060 Ry. To determine the actual energy cut-off value, observing the following table, containing the actual values of the calculation, will provide the necessary information.

Kinetic energy cut-off in [Ry]	Total energy in [Ry]
20	-4754.47890061
40	-5018.40004127
60	-5056.57135901
80	-5060.09198378
100	-5060.22432442
120	-5060.22515892

Table 1: Values of energy cut off and total energy used to plot figure 11.

The results from the calculations are really close to the value of -5060 Ry. Since the numbers after the decimal point don't matter much, the energy cut-off of 80eV will be set as the kinetic energy cut off in all further calculations. The values of 100eV and 120eV would only provide a slightly better result, the time consumed by the calculation would increase drastically.

5.2.2 Automatic k-points

The next step is to look at the convergence in the automatic k-point calculation. The automatic k-points define the grid, that is used to calculate the total energy. Increasing the number of k-points means, that the points in the grid increase as well. The grid is, what defines a discrete integral, that is used to calculate the total energy. By adding more k-points the grid becomes more dense and the calculation of the total energy becomes more accurate.

```
K_POINTS automatic
10 5 3 0 0 0
```

Figure 12: The automatic k-points in the input file. The left three numbers create a so called Monkhorst-Pack grid, the three number on the right indicate an offset of the grid in x y and z direction.

The figure above shows the input for the automatic k-point calculation in an SCF input file. The first three parameters are used to create the grid, while the last three are used for the offset of the grid. The offset wasn't used for any calculation in this thesis and was therefore always 0. The parameters used to change the grid had to be altered, to do the test for convergence. The next figure shows the total energy of the calculation relative to the increase, of the leftmost number in the figure above.

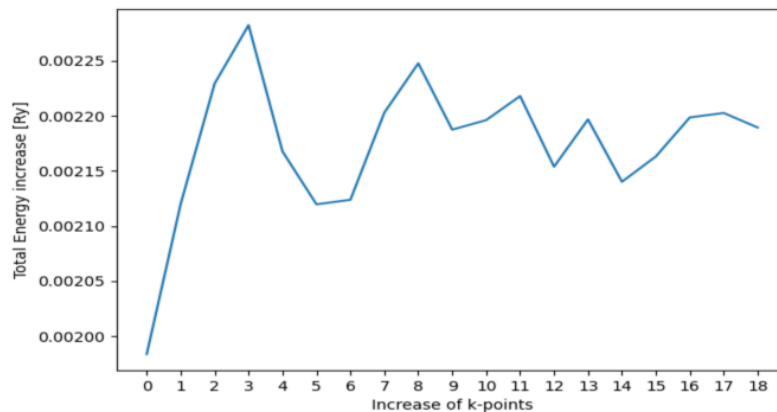


Figure 13: Calculated convergence of the automatic k-points. The figure doesn't show a real convergence and needs to be redone.

The figure doesn't really show any usable convergence behavior. The reason might be, that due to the change in the grid, the calculation didn't work properly. A solution to fix this would be to increase all of the three numbers using the same factor, but due to the number of k-points added in this configuration, the calculation would take a very long time, which wasn't possible to do at this stage of the thesis, because there was not enough

time. The changes in the total energy relative to the change that happens in the energy cut off convergence calculation are way smaller and don't really have to be considered. Therefore the configuration from figure 12 is utilized in all further calculations. Even though the result in this calculation was not a success, from the work in other papers it is known, that a convergence does happen and that the change in energy is really small.

5.3 Pseudopotential

A pseudopotential is a potential that is used in DFT calculations to simplify them. They act as a replacement for complicated interactions. Especially core electrons, that are not relevant for the DFT calculations are replaced with a repulsive potential. Even though pseudopotentials are only a approximation to the real potential, the results of the-DFT is accurate, but takes nowhere as much time and computing power as using the real potential [11].

The pseudopotential used for the calculations in this thesis is called: PBE_NC_FR. It was created by D.R. Hamann. The pseudopotential is fully relativistic, norm-conserving and supports spin-orbit coupling, which means that it is suitable for the calculations performed in this thesis.

The choice was between this pseudopotential and four others. Because of some trouble in the calculations, the other potentials did not work in the beginning, which resulted in the the explicit use of the PBE_NC_FR pseudopotential without any physical based advantage on the other pseudopotentials.

After doing a lot of the calculations in this thesis, the other pseudopotentials eventually worked. Changing the potential at that time would have meant, that all calculations had to be redone. That's why the pseudopotential remained the PBE_NC_FR pseudopotential. Observing the bandstructures of the different pseudopotentials provides no qualitative difference between them apart from a different Fermi energy. Since the Fermi energy is set as 0eV point in every calculation this difference is negligible as well.

Redoing all calculations with a different pseudopotential would be possible, but a change in the results is not to be expected.

5.4 Band structure and spin-orbit coupling

Since spin-orbit coupling is a central aspect of this thesis this section's subject is to find out if spin-orbit coupling is even relevant in the bandstructure of Td-MoTe₂. To do that, two different calculations are performed. In the first calculation, the spin-orbit interaction is disabled in both the scf and nscf calculation.

```
&SYSTEM
  degauss = 0.02
  ecutwfc = 80
  ecutrho = 600
  ibrav = 0
  nat = 12
  nosym = .false.
  ntyp = 2
  occupations = 'smearing'
  smearing = 'cold'
  lspinorb = .true.
  noncolin = .true.
```

Figure 14: Toggling spin-orbit coupling in the input file

The first plot was calculated with the spin-orbit-interaction disabled.

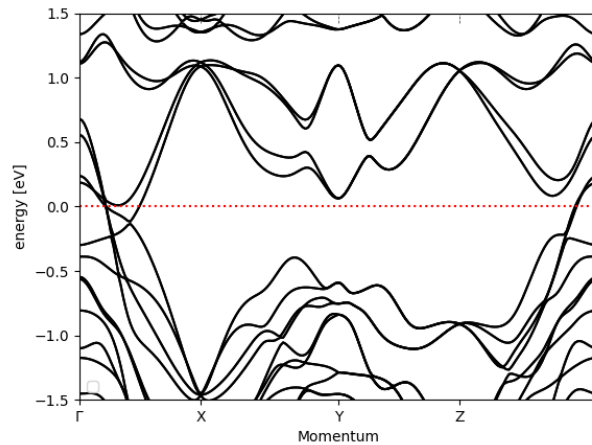


Figure 15: Bandstructure plot with spin-orbit coupling disabled.

The second plot is the calculation but with spin-orbit coupling enabled. At first it might seem like there is no difference, but close to the high symmetry points there is a slight difference visible. Especially around the Γ -Point the plot with spin-orbit coupling can easily distinguished from the plot without.

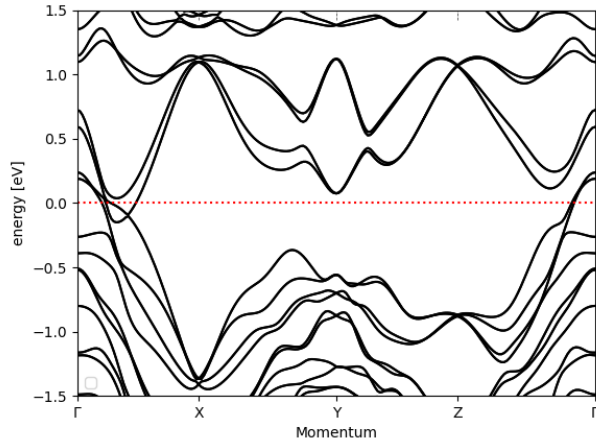


Figure 16: Bandstructure plot with spin-orbit coupling enabled.

To get a better understanding of what is happening, the bandstructure between the Γ - and X-point but especially at the Γ -point around the Fermi energy, is zoomed. Looking at the next figure, we see a lot of bandcrossing, a section where the bands get really close to each other and look like they are crossing each other. The bandcrossing is especially obvious at the Fermi energy on the left and above at 0.05eV .

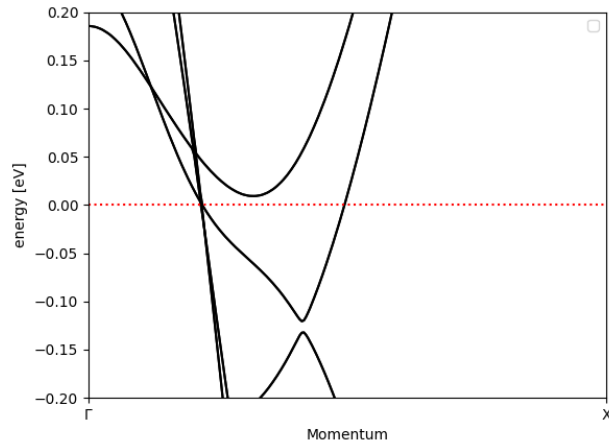


Figure 17: Bandstructure plot close up with spin-orbit coupling disabled.

Comparing the bandstructure with spin orbit coupling in the next figure, with the figure from before we can see, that the bands are not as close to each other and look smoother. The reason for this to happen is, that the spin-orbit coupling causes a splitting of the bands, which leads to a separation of the bands.

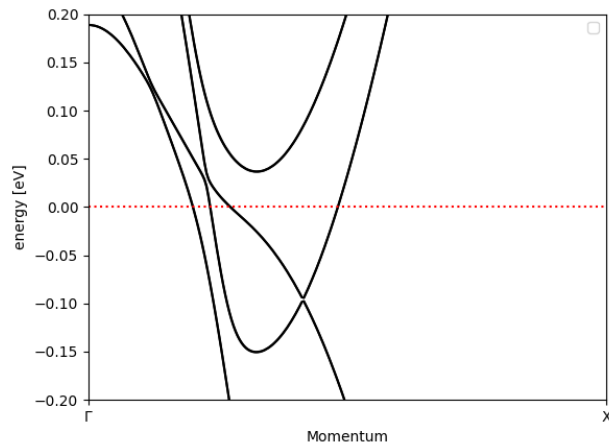


Figure 18: Bandstructure plot close up with spin-orbit coupling enabled.

Looking back at the results, there are clear indications of the spin-orbit coupling having an effect on the bandstructure, as well as fulfilling our expectations of a splitting of the bands. This means the calculations are in good agreement with the theoretical expectations. Although see the effects of the spin-orbit coupling are clearly visible, they are only visible on a relatively small scale.

5.5 Intensities of the bands

The theoretical approach on electron bandstructure models is mostly a model using a certain value for the energy for each k-point in the path that is selected. This approach is very common and the difference between the bands is very clear to see. Small changes in the bandstructure caused by different influences can be detected very easily. Although the approach has many advantages, it doesn't exactly replicate the bandstructure that we can see in experimental results. As shown in the figure below, in actual experimental results the bands aren't lines, but thick bands with higher intensities in the inner part and lower intensities in the outer parts.

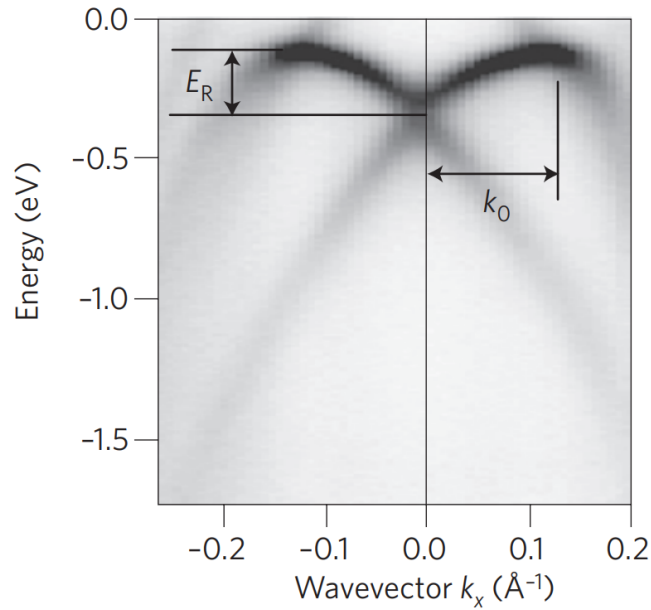


Figure 19: Experimental bandstructure has different intensities in energy values. The intensities serve as a reference for the next steps. This figure was taken from reference [10]

In experiments we see a distribution of the energy around a certain value, that should be the same as the exact value in the calculated bandstructure models. To recreate this distribution the Lorentzian function has the properties that matches the properties of the bandstructure intensities. The Lorentzian function is give by:

$$L(\omega) = \frac{1}{\pi} \frac{\frac{1}{2}\Gamma}{(\omega - \omega_0)^2 + (\frac{1}{2}\Gamma)^2} \quad (59)$$

A basic plot of this function is shown in the next figure.

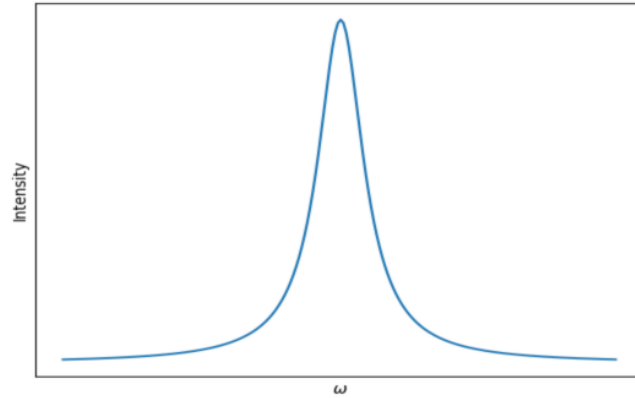


Figure 20: This figure shows the basic course of a Lorentzian function.

Using the Lorentzian function and applying it on the bandstructure, results in the bandstructure shown in the next figure. The bands are broadened and the intensities have the same characteristics like in the experimental result.

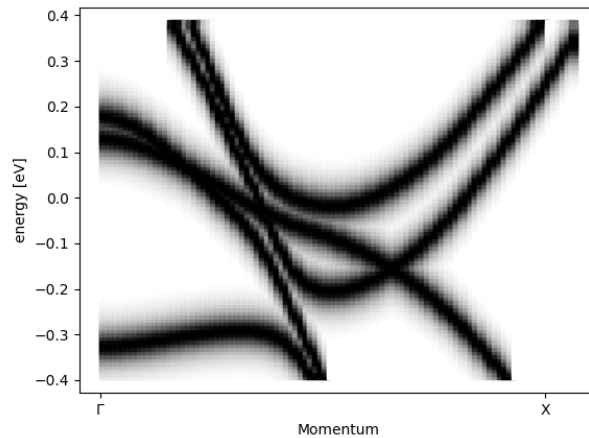


Figure 21: The Lorentzian function is applied on the bandstructure. The bandstructure contains an intensity distribution, comparable to figure 19.

Even though a more realistic plot of the bands was acquired, it is almost impossible to get any information on any properties of the bands that are in the range of a few meV or less.

5.6 Effect of displacement

Looking back at the motivation from the beginning, in the experiment a laser was used to stimulate the phonons in the crystal, to create an innerlayer-shear-mode-excitation. To simulate the experiment we need the phonon excitation. This can be easily done by shifting all atoms in a layer into x or y direction. The shift for this calculation was done in x-direction in intervals of 0.01 angstrom to a maximum of 0.1 angstrom . Figure 22 shows the relative crystal coordinates of the normal calculation without any shifting applied. In figure 23 the full shift of 0.1angstrom is

```
ATOMIC_POSITIONS (crystal)
Mo      0.0000000000    0.5701523176    0.5013961886
Mo      0.5000000000    0.9309408452    0.5137274089
Te      0.0000000000    0.8292326088    0.6405151738
Te      0.5000000000    0.3203379583    0.6024614972
Te      0.5000000000    0.6718554799    0.3746389341
Te      0.0000000000    0.1807587139    0.4127051352
Mo      0.5000000000    0.4298463042    0.0013940924
Mo      0.0000000000    0.0690583638    0.0137264059
Te      0.5000000000    0.1707706309    0.1405141447
Te      0.0000000000    0.6796630124    0.1024598490
Te      0.5000000000    0.8192425895    0.9127041416
Te      0.0000000000    0.3281411755    0.8746370283
```

Figure 22: Position of the atoms in the input file in the base configuration. No displacement was made.

```
ATOMIC_POSITIONS (crystal)
Mo      0.0000000000    0.5701523176    0.5013961886
Mo      0.5000000000    0.9309408452    0.5137274089
Te      0.0000000000    0.8292326088    0.6405151738
Te      0.5000000000    0.3203379583    0.6024614972
Te      0.5000000000    0.6718554799    0.3746389341
Te      0.0000000000    0.1807587139    0.4127051352
Mo      0.5288474147    0.4298463042    0.0013940924
Mo      0.0288474147    0.0690583638    0.0137264059
Te      0.5288474147    0.1707706309    0.1405141447
Te      0.0288474147    0.6796630124    0.1024598490
Te      0.5288474147    0.8192425895    0.9127041416
Te      0.0288474147    0.3281411755    0.8746370283
```

Figure 23: Position of the atoms in the input file in the base configuration. A displacement was applied on the bottom half of the list of atoms. The displacement is 0.1angstrom

After applying the shift on the calculations, one specific band in the bandstructure, marked red in the next figure is observed.

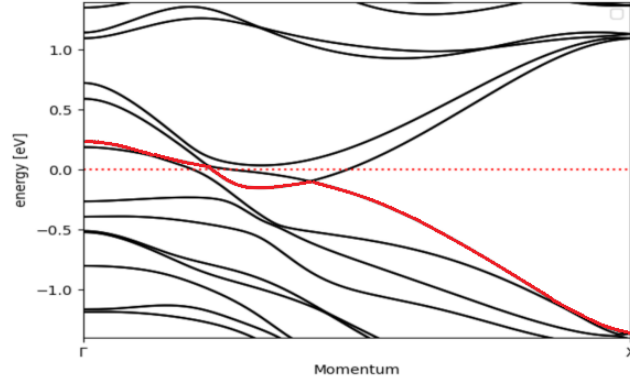


Figure 24: The red marked band in the bandstructure is the one that was observed in the displacement process.

The calculated band without any displacement of the atoms applied, serves as a reference for the following calculations. The calculated bands with the shift applied are now subtracted by the reference band without any shift. This results in plots indicating energy increase and energy decrease. The results of these calculations is shown in the next figure. Because of visual reasons only every second band is considered in this plot.

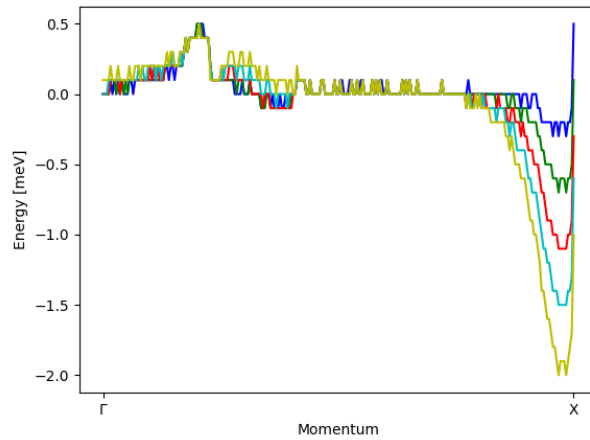


Figure 25: The figure shows the change in energy of the bands that underwent a displacement compared to the band without displacement. The color of the plotted functions belong to the following displacements:

color	displacement
blue	0.02 angstrom
green	0.04 angstrom
red	0.06 angstrom
turquoise	0.08 angstrom
yellow	0.10 angstrom

There are only very small changes in energy. The changes are very small close to the Γ -point but very clear to see around the X-point. The energy at the X-point decreases by around 0.2meV-0.6meV for every 0.2angstrom of displacement. The maximum decrease is 2meV at a displacement of 0.1angstrom of the atoms. Since a shift in the bandstructure was expected, a satisfying result was achieved. The change happens due to a change in symmetry, which means, that the spin-orbit coupling which is directly related to the symmetry is probably the cause for the change in energy. Looking at figure 16, the bands are very close to each other around the X-point, while the band, that was observed during the displacement, is the top most of the bands at the X-point. The change in symmetry and the lowering of the spin-orbit coupling effect results in a lesser strong splitting of the bands, the observed and the other bands at the X-point get closer to each other, resulting in a lesser energy of the observed band. Also the energy of 2meV is close to the energies that were measured, which were also only a few meV. The simulation of the interlayer-sheer-mode-excitation by displacing the atoms was therefore successful.

6 Conclusion/Outlook

Now it can be concluded, what was achieved in this thesis and the the next steps, that would be appropriate to take, to further investigate the influence of spin-orbit coupling on the electronic properties of Molybdenum ditelluride, can be discussed.

First of all the convergence calculation for the cut-off parameter was a success, a good value was identified and the convergence was easy to see.

The convergence calculation for the automatic k-points on the other hand was not as successful. The convergence was not really visible and therefore the values have a poor accuracy. Nevertheless, it was obvious, that changing the grid density, doesn't influence the total energy too much and from other sources it is known, that the automatic k-point calculation always converges. Therefore the base set of automatic k-points was utilized to to any further calculations.

The test if spin-orbit coupling has an impact on the electron bandstructure of the Td-MoTe₂ was also successful. The bandstructure without spin-orbit-coupling has a lot of bandcrossings, that can easily identify and in the bandstructure with spin-orbit-coupling these crossings are separated due to spin splitting. Therefore the bands look smoother and the expected result was verified.

To get a more realistic bandstructure in terms of intensities, the Lorentzian function was applied and resulted in a bandstructure, that, in terms of intensities, is relativley close, to what it should look like. The calculation can be altered and applied to any bandstructure calculation. The only downside is, that the ability to observe small changes is lost and therefore calculations like the previous one wouldn't be as easy to perform.

The last part of the research was supposed to replicate the inner-layer-sheer-mode-excitation from the motivation. By displacing the atoms along in one direction for a certain amount, changes in the bandstructure were clearly visible. These changes had a similar magnitude, just like the changes in the experiment. Therefore the method was a success and can be applied to simulate a phonon excitation.

The next step in this subject would be to redo the automatic k-point convergence calculation to prove, that the total energy converges for increasing the k-points.

After that, the displacement could be further investigated. Since MoTe₂ should have a 1T'-MoTe₂ state just like WTe₂ the method of phonon excitation could be used and compared to the 1T'-MoTe₂. When the bandstructure with the phonon excitation exactly matches the 1T'-MoTe₂ bandstructure the amount of displacement needed, to reach the structural phase transition, would be received. Another idea could be to do the experiment from the motivation, but with MoTe₂ instead of WTe₂ and compare the actual results to the prognosis that was done in this thesis.

7 References

References

- [1] Hein, P., Jauernik, S., Erk, H. et al. Mode-resolved reciprocal space mapping of electron-phonon interaction in the Weyl semimetal candidate Td-WTe₂. *Nat Commun* 11, 2613 (2020). <https://doi.org/10.1038/s41467-020-16076-0>
- [2] Mao, D., Du, B., Yang, D., Zhang, S., Wang, Y., Zhang, W., She, X., Cheng, H., Zeng, H. and Zhao, J. (2016), Nonlinear Saturable Absorption of Liquid-Exfoliated Molybdenum/Tungsten Ditelluride Nanosheets. *Small*, 12: 1489-1497. <https://doi.org/10.1002/sml.201503348>
- [3] P. Hohenberg and W. Kohn: Inhomogeneous Electron Gas. *Phys. Rev.* 136 (1964) B864-B871, doi:10.1103/PhysRev.136.B864
- [4] Giustino, Feliciano. *Materials Modelling Using Density Functional Theory : Properties and Predictions*, Oxford University Press, 2014. ProQuest Ebook Central, <http://ebookcentral.proquest.com/lib/christianalbrechts/detail.action?docID=1688422>
- [5] Kopitzki K., Herzog, P., *Einführung in die Festkörperphysik*, Springer-Verlag GmbH Deutschland, 2017
- [6] Kim, Dae Mann. *Introductory Quantum Mechanics for Applied Nanotechnology*, John Wiley & Sons, Incorporated, 2015
- [7] Dresselhaus, M.S., Dresselhaus, G., Jorio, A.. *Group Theory: Application to the Physics of Condensed Matter*, 337,(2008)
- [8] Winkler R.. *Spin–Orbit Coupling Effects in Two-Dimensional Electron and Hole Systems*, p.69 ff., (2003)
- [9] Lechner, V. *Bulk and Structure Inversion Asymmetry in Semiconductor Quantum Well Structures*, 9, (2012)
- [10] Manchon, A., Koo, H., Nitta, J. et al. New perspectives for Rashba spin–orbit coupling. *Nature Mater* 14, 872 (2015). <https://doi.org/10.1038/nmat4360>
- [11] Schwerdtfeger, P. (2011), The Pseudopotential Approximation in Electronic Structure Theory. *ChemPhysChem*, 12: 3143-3155. <https://doi.org/10.1002/cphc.201100387>
- [12] Dresselhaus, G. Spin-orbit coupling effects in zinc blende structures. *Phys. Rev.* 100, 580–586 (1955)

- [13] Rashba, E. Properties of semiconductors with an extremum loop. 1. Cyclotron and combinational resonance in a magnetic field perpendicular to the plane of the loop. *Sov. Phys. Solid State* 2, 1109–1122 (1960)

8 Appendix

8.1 Basic SCF input file

```
&CONTROL
  calculation = 'scf'
  etot_conv_thr = 1.2000000000d-12
  forc_conv_thr = 1.0000000000d-06
  outdir = './out/'
  prefix = 'wte2'
  pseudo_dir = "/gxfs_work1/cau/supas414/pseudopotentials/PBE_NC_FR"
  tpmfor = .true.
  tstress = .true.
  verbosity = 'high'
/
&SYSTEM
  degauss = 0.02
  ecutwfc = 80
  ecutrho = 600
 ibrav = 0
  nat = 12
  nosym = .false.
  ntyp = 2
  occupations = 'smearing'
  smearing = 'cold'
  lspinorb = .true.
  noncolin = .true.
/
&ELECTRONS
  conv_thr = 1.000000000d-12
  mixing_beta = 4.000000000d-01
/
&ions
  ion_dynamics = 'bfgs'
  ! bfgs_ndim = 2
  upscale = 1
  trust_radius_max = 0.2
  trust_radius_min = 1.00D-4
  trust_radius_ini = 0.2
/
&cell
  cell_dynamics = 'bfgs'
  cell_dofree = 'xyz'
/
ATOMIC_SPECIES
Te 127.6 Te.upf
Mo 95.95 Mo.upf
K_POINTS automatic
10 5 3 0 0 0
CELL_PARAMETERS (angstrom)
  3.466515142 0.000000000 0.000000000
  0.000000000 6.382674179 0.000000000
  0.000000000 0.000000000 15.660302313
ATOMIC_POSITIONS (crystal)
Mo 0.000000000 0.5701523176 0.5013961886
Mo 0.500000000 0.9309408452 0.5137274089
Te 0.000000000 0.8292326088 0.6405151738
Te 0.500000000 0.3203379583 0.6024614972
Te 0.500000000 0.6718554799 0.3746389341
Te 0.000000000 0.1807587139 0.4127051352
Mo 0.500000000 0.4298463042 0.0013940924
Mo 0.000000000 0.0690583638 0.0137264059
Te 0.500000000 0.1707706309 0.1405141447
Te 0.000000000 0.6796630124 0.1024598490
Te 0.500000000 0.8192425895 0.9127041416
Te 0.000000000 0.3281411755 0.8746370283
```

8.2 Basic NSCF input file

```
&CONTROL
  calculation = 'nscf'
  etot_conv_thr = 1.2000000000d-12
  forc_conv_thr = 1.0000000000d-06
  outdir = './out/'
  prefix = 'vrte2'
  pseudo_dir = "/gxfs_work1/cau/supas414/MoTe2/pseudopotentials/PBE_NC_FR"
  tprnfor = .true.
  tstress = .true.
  verbosity = 'high'
/
&SYSTEM
  degauss = 0.02
  ecutwfc = 80
  ecutrho = 600
  ibrav = 0
  nat = 12
  nosym = .false.
  ntyp = 2
  occupations = 'smearing'
  smearing = 'cold'
  lspinorb = .true.
  noncolin = .true.
/
&ELECTRONS
  conv_thr = 1.000000000d-10
  mixing_beta = 4.000000000d-01
/
&ions
  ion_dynamics = 'bfgs'
  ! bfgs_ndim = 2
  upscale = 1
  trust_radius_max = 0.2
  trust_radius_min = 1.00D-4
  trust_radius_ini = 0.2
/
&cell
  cell_dynamics = 'bfgs'
  cell_dofree = 'xyz'
/
ATOMIC_SPECIES
Te 127.6 Te.upf
Mo 95.95 Mo.upf
K_POINTS crystal_b
2
0.0 0.0 0.0 250 #Gamma
0.5 0.0 0.0 250

CELL_PARAMETERS (angstrom)
3.466515142 0.000000000 0.000000000
0.000000000 6.382674179 0.000000000
0.000000000 0.000000000 15.660302313
ATOMIC_POSITIONS (crystal)
Mo 0.000000000 0.5701523176 0.5013961886
Mo 0.500000000 0.9309408452 0.5137274089
Te 0.000000000 0.8292326088 0.6405151738
Te 0.500000000 0.3203379583 0.6024614972
Te 0.500000000 0.6718554799 0.3746389341
Te 0.000000000 0.1807587139 0.4127051352
Mo 0.500000000 0.4298463042 0.0013940924
Mo 0.000000000 0.0690583638 0.0137264059
Te 0.500000000 0.1707706309 0.1405141447
Te 0.000000000 0.6796630124 0.1024598490
Te 0.500000000 0.8192425895 0.9127041416
Te 0.000000000 0.3281411755 0.8746370283
```

8.3 Code used to calculate the bandstructure with intensities

```
import numpy as np
import matplotlib.mlab as mlab
import matplotlib.pyplot as plt
import matplotlib.gridspec as gs
import matplotlib
import sys
import Lorentz
from PIL import Image
#Loading the datafile bands.out.gnu
f = np.loadtxt('bands.out.gnu')
l = []
k = []
fermi = 11.6140
for i in range(0,len(f)-1):
    f[i,l] = f[i,l]-fermi
    if f[i,l] > -0.4 and f[i,l] < 0.4:
        l.append(f[i,l])
        k.append(f[i,0])
mink = min(k)
maxk = max(k)
maxl = max(l)
minl = min(l)
resolution = 100
print(maxl)
print(minl)
print(k)
intervall = (maxl-minl)/resolution
intervalk = (maxk-mink)/resolution
graph = []
grid = []
for i in range (0,resolution-1):
    grid.append([])
    for j in range (0,resolution-1):
        grid[i].append(0)

for i in range(0,len(l)-1):
    graph.append(Lorentz.Lorentz(0.03,l[i]))
norm = []
for i in range(0,len(l)-1):
    norm.append(max(graph[i][1]))
    norm.append(min(graph[i][1]))

intmax = max(norm)
intmin = min(norm)
normfac = intmax-intmin
```

```

for i in range(0,len(graph)):
    for j in range(0,len(graph[i][1])):
        graph[i][1][j] = (graph[i][1][j]-intmin)/normfac

for i in range(0,len(grid)):
    for t in range(0,len(k)-1):
        if k[t] >= (intervalk*i) and k[t] <=
(intervalk*i+intervalk):
            for j in range(0,len(grid)):
                find_max = []
                for q in range(0,len(graph[i][0])-1):
                    if graph[t][0][q] >=
(minl+j*intervall) and graph[t][0][q] <=
(minl+j*intervall+intervall):
                        grid[i][j].append(graph[t][1]
[q])

for i in range (0,resolution-1):
    for j in range (0,resolution-1):
        grid[i][j] = max(grid[i][j])
print(grid)

for i in range(0,len(grid)-1):
    for j in range(len(grid)-1):

        plt.plot((intervalk*i+intervalk/2), (minl+j*intervall+inte
rvall/2), 's', color = str(1-grid[i][j]), alpha = 1.0)

#im = Image.new("RGB", (resolution,resolution), (0,0,0))
#for i in range(0,resolution-1):
#    for j in range(0,resolution-1):
#        im.paste((round(grid[i][j]*256),0,0), (i,j,i+1,j+1))
#im.show()

#for i in range(0,len(graph)-1):
#    for j in range(0,len(graph[i][0])-1):
#        plt.plot(k[i],graph[i][0][j], 't**2', color=str(1-
(graph[i][1][j]-1.5)/2))
#
plt.xticks([0,0.308], ['$\Gamma$', 'X'])
plt.ylabel('energy [eV]')
plt.xlabel('Momentum')
plt.show()
#print(graph)

import numpy as np
import matplotlib.mlab as mlab
import matplotlib.pyplot as plt
import matplotlib.gridspec as gs
import sys
def Lorentz(width,energy):
    retv = [[],[]]
    l = []
    eV = []
    for i in range(0,200):
        eV.append(energy-0.1+0.001*i)
    for i in range(0,200):
        l.append((1/np.pi)*width/((eV[i]-energy)*(eV[i]-
energy)+width*width))
    retv[0] = eV
    retv[1] = l
    return retv

```

9 Selbstständigkeitserklärung

Hiermit erkläre ich, dass ich diese Bachelorarbeit selbständig verfasst habe und keine anderen als die angegebenen Quellen und Hilfsmittel benutzt habe. Darüber hinaus erkläre ich, dass die vorliegende Arbeit noch nicht im Rahmen eines anderen Prüfungsverfahrens an dieser oder einer anderen Hochschule eingereicht wurde.

Kiel, den

(Neil Henrik Matzen)